

Longitudinal-Transverse Separation of the Deuterium ($e, e'p$) Response Functions

M. van der Schaar,⁽¹⁾ H. Arenhövel,⁽²⁾ Th. S. Bauer,⁽¹⁾ H. P. Blok,^{(3),(4)} H. J. Bulten,⁽³⁾ M. Daman,⁽³⁾ R. Ent,^{(4),(a)} E. Hummel,⁽⁵⁾ E. Jans,⁽³⁾ G. J. Kramer,^{(3),(b)} J. B. J. M. Lanen,⁽¹⁾ L. Lapikás,⁽³⁾ J. H. Mitchell,^{(4),(c)} G. van der Steenhoven,⁽³⁾ J. A. Tjon,⁽⁵⁾ P. K. A. de Witt Huberts,^{(1),(3)} and A. Zondervan⁽³⁾

⁽¹⁾*Department of Nuclear Physics, Rijksuniversiteit Utrecht, P.O. Box 80.000, 3508 TA Utrecht, The Netherlands*

⁽²⁾*Institut für Kernphysik, Johannes Gutenberg-Universität, D-6500 Mainz, Federal Republic of Germany*

⁽³⁾*Nationaal Instituut voor Kernfysica en Hoge-Energiefysica, P.O. Box 41882, 1009 DB Amsterdam, The Netherlands*

⁽⁴⁾*Department of Physics, Vrije Universiteit, Amsterdam, The Netherlands*

⁽⁵⁾*Institute for Theoretical Physics, Rijksuniversiteit Utrecht, P.O. Box 80.006, 3508 TA Utrecht, The Netherlands*

(Received 13 December 1990)

In the four-momentum-transfer range $0.05 \leq q^2 \leq 0.27$ (GeV/c)², longitudinal and transverse response functions have been determined by performing a Rosenbluth separation of ${}^2\text{H}(e, e'p)$ coincidence cross sections measured in parallel kinematics. The results are compared to nonrelativistic calculations that include the effects of final-state interaction, meson-exchange currents, and isobar configurations, and to relativistic calculations that include the effects of final-state interaction. The ratios of the response functions agree with both calculations; the absolute values are $(16 \pm 3 \pm 8)\%$ larger than predicted.

PACS numbers: 25.30.Fj, 25.10.+s, 27.10.+h

The deuteron system plays an essential role in nuclear physics as this bound two-nucleon system contributes to the basis of our understanding of the nucleon-nucleon interaction, being the microscopic input for any fundamental model of heavier nuclei. In the theoretical calculations of the two-nucleon system the state of the art is such that experiments with high precision are important to enable comparisons with theoretical predictions and possibly distinguish between the various calculations. The level of our understanding of the two-nucleon system is illustrated by the reasonable description of many existing electron-scattering data.¹⁻³ Only a limited set of high-precision exclusive experiments exists. In particular, no exclusive experiments aimed at separating individual structure functions of the deuteron in the quasielastic domain have been reported so far. Given its general interest, it is of relevance to obtain such precise exclusive data on the deuteron electrodisintegration process. These data should preferably involve the coincident ($e, e'p$) reaction as it gives access to four independent observables (if no polarization degrees of freedom are considered).

In the past, several inclusive quasielastic (QE) electron-scattering experiments have been performed on the deuteron. Nonrelativistic calculations show good agreement with the separated inclusive longitudinal and transverse response functions⁴ in the three-momentum-transfer range between 300 and 500 MeV/c. In exclusive experiments the cross sections are measured over a large missing-momentum range,^{5,6} and are rather well reproduced by nonrelativistic calculations. In this paper we present the results of an exclusive ${}^2\text{H}(e, e'p)$ experiment, in which both the longitudinal and transverse response functions have been determined.

The description of the QE ($e, e'p$) process is generally based on the following assumptions: (i) A simple virtual photon is involved in the knockout process (one-photon-exchange approximation); (ii) the energy and momentum that the electron loses in the scattering process are transferred to a single nucleon (quasielastic-scattering process); (iii) for the nucleon current the free-nucleon current is taken, modified for off-shell effects [impulse approximation (IA)]. In order to investigate the validity of these assumptions, experiments have been performed on several nuclei, e.g., ${}^4\text{He}$ (Refs. 7 and 8), ${}^6\text{Li}$ (Ref. 9), ${}^{12}\text{C}$ (Refs. 10 and 11), and ${}^{40}\text{Ca}$ (Refs. 12 and 13) at various laboratories. For nuclei with $A > 3$ no exact microscopic calculations of the nuclear dynamics are available at present, which implies that additional assumptions are needed in the interpretation of these data, especially on the treatment of the final-state interaction (FSI). Only for the lightest systems ($A \leq 3$) do exact calculations exist.^{1,14-16} Differences between these calculations are due to the N - N interaction employed, the (non)relativistic character, and/or the theoretical method employed. In the case of deuterium, various calculations are available^{14,17} that are all essentially based on the assumptions mentioned above. Hence a quasielastic ${}^2\text{H}(e, e'p)$ experiment is well suited to study these assumptions.

In our comparison with the data we will use both relativistic (R) and nonrelativistic (NR) calculations. The essential difference between the two calculations is that in the R calculations both the nucleon current operator and the wave function are completely relativistic.¹⁷ Moreover, the NR and R calculations make use of different deuteron wave functions (Paris¹⁸ and Blankenbecker-Sugor-Logunov-Tavkhelidze¹⁹) and different nu-

cleon form factors (dipole with $G_E^n=0$ and Höhler *et al.*,²⁰ respectively). However, as can be seen from detailed comparisons between various combinations in Ref. 3, no large effects on the observables in our kinematical domain due to these differences are to be expected. FSI effects are included in both types of calculations, including charge-exchange contributions. The NR calculations¹⁴ include effects that go beyond the impulse approximation, i.e., meson-exchange currents (MEC) and isobar contributions (IC) have been included.

The coincidence cross section for electrodisintegration of the deuteron contains four structure functions f_{00} , f_{11} , f_{01} , and f_{-11} which depend on the energy of the relative motion ($E_{np}^{c.m.}$) of the final np state, the three-momentum-transfer squared q^2 , and the angle $\theta_{np}^{c.m.}$. Explicit definitions of the cross section and the structure functions $f_{\mu\mu'}$ are given in Ref. 14. The information on the dynamics of the two-nucleon system is contained in the four structure functions $f_{\mu\mu'}$. In principle, the strongest test of the theory is to experimentally separate f_{00} , f_{11} , f_{01} , and f_{-11} , and compare them directly to the model predictions. Such a separation would require out-of-plane measurements, which is experimentally very difficult. As a first step we have carried out in-plane measurements in parallel kinematics in which the emitted proton momentum \mathbf{p}' is parallel to \mathbf{q} . In these kinematics the interference structure functions f_{01} and f_{-11} vanish.¹⁴ The remaining two structure functions (f_{00} and f_{11}) can then be obtained from the measured cross sections by a standard Rosenbluth separation. As one of the aims of this study is an investigation of the validity of the IA, we use the ratio of f_{11} and f_{00} , in which the uncertainties due to the nuclear wave function cancel, as well as most of the systematic uncertainties. We will represent the experimental data both in terms of the structure functions and by the ratio

$$R_G = \left[\frac{2m^2/q^2}{f_{11}/f_{00}} \right]^{1/2},$$

with m the proton mass. In the plane-wave impulse approximation (PWIA), R_G is, apart from off-shell effects, equal to G_M^p/G_E^p , the ratio of the magnetic and electric proton form factors. A deviation of the experimentally found ratio from the PWIA prediction will then be a signature of contributions due to FSI effects or of a breakdown of the IA, due to, for instance, two-body currents. The absolute separated structure functions will provide information on both the validity of the aforementioned assumptions and the employed deuteron wave functions.

The experiment was performed at the medium-energy electron accelerator MEA of NIKHEF-K, using typical beam currents of 10 μ A. The two high-resolution magnetic spectrometers at NIKHEF-K allow a precise determination of the electron and proton angles and momenta.²¹ A deuterium target of the waterfall type²² was used with heavy water $^2\text{H}_2\text{O}$. The waterfall was sur-

rounded by stainless-steel walls of 10 μ m allowing a 0.3-bar atmosphere of helium to keep the water in the liquid state. The walls were outside the coincidence acceptance of the spectrometers. The target angle could be chosen freely, but changes were few in order to keep systematic uncertainties in the target thickness as small as possible. In Table I the kinematics corresponding to the central settings of the spectrometers are given. The measured target thicknesses are also listed.

Since the liquid target is subject to thickness variations, knowledge of these variations is crucial for the relative normalization between the various measurements. The target thickness, which is related to the pumping speed of the target system, was determined and controlled in different, partly overlapping ways. The thickness was calibrated by measuring elastic- and inelastic-scattering cross sections off ^2H and ^{16}O . Fourier-Bessel coefficients were used to calculate cross sections for elastic scattering off ^{16}O (Ref. 23) and for the excitation of the 3^- state at 6.13 MeV.²⁴ For ^2H we determined Fourier-Bessel coefficients from $^2\text{H}(e,e)$ elastic cross sections²⁵ measured at three incident beam energies (300, 500, and 650 MeV). The present elastic-scattering measurements were performed at least once for each beam energy used.²⁶ The statistical error in the given target thicknesses is about 1%. These data, in conjunction with elastic- and inelastic-scattering data on boron-nitride and tantalum targets, provided a good beam energy calibration accurate to 200 keV.

In order to continuously monitor the target thickness, the prompt trigger rates of the detection systems in both spectrometers were used to obtain ratios of triggers to integrated charge. By changing the angle and field setting of only one spectrometer at a time, while the other spectrometer remained unchanged, the target thickness could

TABLE I. Kinematics and target thickness t of $^2\text{H}(e,e'p)n$ measurements. k_{lab} is the incoming electron energy, θ_e is the electron-scattering angle, p_m is the missing momentum ($p_m = q - p'$), q the three-momentum transfer, and ω is the transferred energy.

k_{lab} (MeV)	θ_e (deg)	p_m (MeV/c)	q (MeV/c)	ω (MeV)	t (mg/cm ²)
296.7	77.10	39.8	329.3	73.1	5.89
296.7	68.75	69.9	299.3	74.8	5.71
296.7	58.10	109.9	259.3	78.6	5.43
296.7	107.39	38.8	418.7	77.0	5.46
555.9	36.04	40.4	328.8	73.1	5.68
555.9	32.55	69.8	299.4	74.8	5.72
524.5	50.10	37.6	417.5	77.0	5.54
524.5	45.68	39.8	380.9	93.1	5.54
524.5	63.24	58.8	503.3	104.1	5.76
524.5	29.56	110.2	259.0	76.7	5.71
350.9	113.43	58.4	502.9	104.0	6.19
298.6	96.37	40.0	380.7	93.1	5.21

be determined for each individual measurement.²⁶ Note that these stepwise changes are not included in Table I. The overall systematic error in the cross sections (5%) is dominated by the uncertainty in the theoretical elastic and inelastic cross sections (2%–3%) and by the proton spectrometer solid angle (2%). The statistical error in the coincidence cross sections is about 1%. The systematic error in R_G ranges between 3.4% and 14%. The systematic error in the separated structure functions can be somewhat larger in unfavorable kinematics. For f_{00} it ranges from 6% to 8% and for f_{11} from 5% to 28%.

Since the acceptances of the spectrometers are finite, each measurement involves a range of p_m , q , and ω values. The acceptance in p_m is typically 30 MeV/c. As an example we show in Fig. 1 the separated structure functions for the measurement centered at $q=299$ MeV/c and $\omega=75$ MeV as a function of p_m . The dotted line represents the R calculation including FSI effects. The calculation needs to be corrected for the effect of the range of q and ω values contributing to one p_m bin. The corrected calculation is represented by the solid line. The NR calculation which includes both the FSI effects and finite-acceptance effects is plotted as the dashed line. The short-dashed line, which is hardly distinguishable from the dashed line, represents the NR calculation also incorporating MEC and IC effects. We conclude that the MEC and IC effects are negligible in this kinematics. The data are well described by both the R and NR cal-

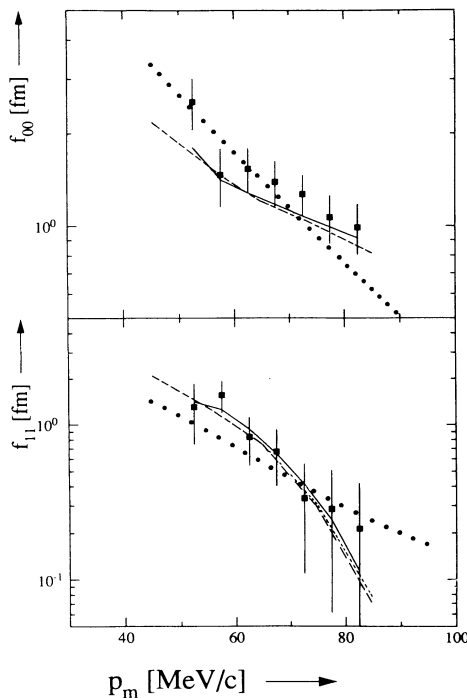


FIG. 1. The separated structure functions as a function of the missing momentum at $q=299$ MeV/c and $\omega=75$ MeV. The meaning of the curves is explained in the text.

culations.

In order to study the overall features of the data, the ratio R_G is calculated for each p_m bin. The resulting R_G values are averaged over all bins contained in one measurement. The results are compared to the calculations which are treated similarly in Fig. 2. R_G is well described by both the NR and the R calculations. The average deviations amount to $(0 \pm 2)\%$ and $(-2 \pm 2)\%$, respectively. Only statistical errors are considered in these ratios. The separated structure functions are plotted in terms of a ratio of measured structure functions and PWIA predictions in Fig. 2. The ratios $f_{00}^{\text{expt}}/f_{00}^{\text{theory}}$ and $f_{11}^{\text{expt}}/f_{11}^{\text{theory}}$ have been averaged over all measurements. For the NR calculations including FSI, MEC, and IC we obtain $1.15 \pm 0.03(\text{stat}) \pm 0.08(\text{syst})$ and $1.17 \pm 0.03 \pm 0.08$. For the R calculations we find $1.12 \pm 0.03 \pm 0.07$ and $1.19 \pm 0.03 \pm 0.09$ for f_{00} and f_{11} , respectively. Hence, we see that the theoretical calculations underestimate the data at the 2σ level. Given the trend of this small discrepancy it will be of interest to extend these measurements to higher momentum

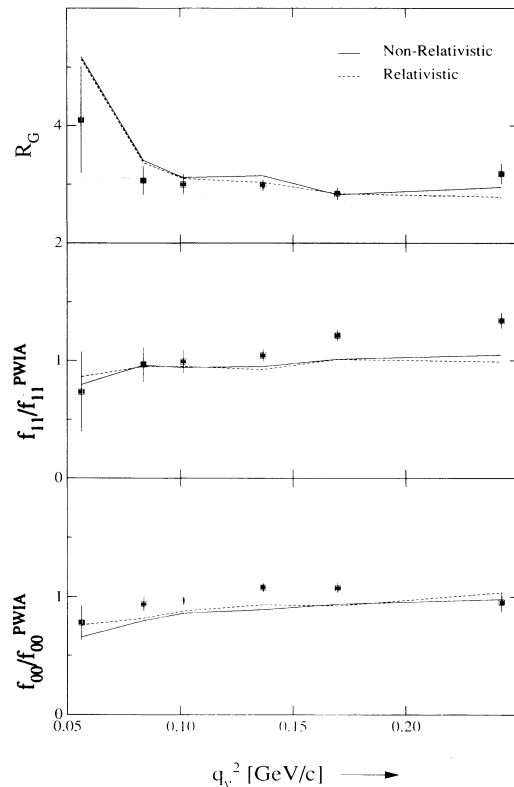


FIG. 2. Longitudinal (f_{00}) and transverse (f_{11}) structure functions for the reaction ${}^2\text{H}(e,e'p)$ as a function of the four-momentum-transfer squared. The top panel shows the quantity R_G . The dotted line is the PWIA calculation (NR). In the middle (lower) panel the ratio of f_{00} (f_{11}) and the PWIA calculation (NR) is displayed. The solid (dashed) line represents the nonrelativistic (relativistic) calculation.

transfer.

In the reaction ${}^2\text{H}(e,e'p)$ no deviation from the impulse approximation is found for the R_G data in the q_v^2 range between 0.05 and 0.27 $(\text{GeV}/c)^2$. This seems to indicate that the elementary assumptions entering the interpretation of the quasifree ${}^2\text{H}(e,e'p)$ data are well in hand. However, an equal modification of both the electric and magnetic nucleon form factors would also result in an agreement between theory and experiment, although such a modification does imply a breakdown of the IA. In fact, a comparison of the f_{00} and f_{11} data to the calculations shows how a small discrepancy between theory and experiment for the individual structure functions does not necessarily lead to a discrepancy for R_G . This conclusion does not depend on the type of calculations used as the two approaches essentially agree in the presently investigated kinematical region. The origin of the 2σ deviation between theory and experiment is unclear.

We would like to thank Dr. J. Friedrich for letting us use the waterfall target, and M. B. Leuschner for his assistance in the installation and operation of the target system. This work is part of the research program of the National Institute for Nuclear and High-Energy Physics (NIKHEF-K), made possible by financial support from the Foundation for Fundamental Research on Matter (FOM) and The Netherlands' Organization for Advancement of Pure Research (NWO).

^(a)Present address: Laboratory for Nuclear Science, MIT, Cambridge, MA 02139.

^(b)Present address: JET Joint Undertaking, Abingdon, Oxfordshire, United Kingdom.

^(c)Present address: University of Virginia, Charlottesville, VA 22901.

- ¹H. Arenhövel, Nucl. Phys. **A384**, 287 (1982).
²J. F. Mathiot, Phys. Rep. **173**, 63 (1989).
³E. Hummel and J. A. Tjon, Phys. Rev. Lett. **63**, 1788 (1989); Phys. Rev. C **42**, 423 (1990).
⁴B. P. Quinn *et al.*, Phys. Rev. C **37**, 1609 (1988).
⁵M. Bernheim *et al.*, Nucl. Phys. **A365**, 349 (1981).
⁶S. Turck-Chieze *et al.*, Phys. Lett. **142B**, 145 (1984).
⁷A. Magnon *et al.*, Phys. Lett. B **222**, 352 (1989).
⁸J. F. J. van den Brand *et al.*, Phys. Rev. Lett. **60**, 2006 (1988).
⁹G. van der Steenhoven *et al.*, Phys. Rev. Lett. **58**, 1727 (1987).
¹⁰G. van der Steenhoven *et al.*, Phys. Rev. Lett. **57**, 182 (1986).
¹¹P. E. Ulmer *et al.*, Phys. Rev. Lett. **59**, 2259 (1987).
¹²D. Reffay-Pikeroen *et al.*, Phys. Rev. Lett. **60**, 776 (1988).
¹³L. Lapikás, in *Proceedings of the Sixth Miniconference on Electron Scattering: Past and Future, Amsterdam, 1989*, edited by C. W. de Jager, E. Jans, L. Lapikás, and H. de Vries (NIKHEF, Amsterdam, 1989), p. 81.
¹⁴W. Fabian and H. Arenhövel, Nucl. Phys. **A314**, 253 (1979).
¹⁵E. van Meijgaard and J. A. Tjon, Phys. Rev. Lett. **61**, 1461 (1988).
¹⁶J. M. Laget, Nucl. Phys. **A312**, 265 (1978).
¹⁷E. Hummel and J. A. Tjon (to be published); the calculations to which we refer here are essentially a generalization of Ref. 1.
¹⁸M. Lacombe *et al.*, Phys. Rev. C **21**, 861 (1980).
¹⁹R. Blankenbecker *et al.*, Phys. Rev. **142**, 1051 (1966).
²⁰C. Höhler *et al.*, Nucl. Phys. **B114**, 505 (1976).
²¹C. de Vries *et al.*, Nucl. Instrum. Methods **249**, 337 (1984).
²²N. Voegler and J. Friedrich, Nucl. Instrum. Methods **198**, 293 (1982).
²³H. de Vries, C. W. de Jager, and C. de Vries, At. Data Nucl. Data Tables **36**, 495 (1987).
²⁴T. N. Butti *et al.*, Phys. Rev. C **33**, 755 (1986).
²⁵S. Platchkov *et al.*, Nucl. Phys. **A510**, 740 (1990).
²⁶M. van der Schaar, Ph.D. thesis, Rijksuniversiteit Utrecht, 1991.